

X-RAY TRANSIENT CDF-S XT2: THE ELECTROMAGNETIC AND GRAVITATIONAL-WAVE RADIATIONS OF A SUPRA-MASSIVE NEUTRON STAR

HOU-JUN LÜ¹, YONG YUAN¹, LIN LAN¹, BIN-BIN ZHANG^{2,3}, JIN-HANG ZOU⁴ AND EN-WEI LIANG¹

ABSTRACT

The merging process of binary neutron stars is the source of the quadrupole gravitational-wave (GW) radiation. Its remnant can be either a supra-massive or a stable NS. Such evidence of magnetar signature has been supported indirectly by observed X-ray plateau of some gamma-ray bursts (GRBs) afterglow. Recently, Xue et al. (2019) discovered an X-ray transient CDF-S XT2 that is claimed to be powered by a stable magnetar from the merger of double NS. In this paper, we revisit the X-ray emission of CDF-S XT2 and find that it is more consistent with a supra-massive magnetar central engine, surviving thousands of seconds to collapse black hole. We present the comparisons of the X-ray plateau luminosity, break time, and the parameters of magnetar between CDF-S XT2 and other short GRBs with internal plateau samples. By adapting the collapse time to constrain the equation of state (EOS), we find that three EOSs (GM1, DD2, and DDME2) are consistent with the observational data. On the other hand, if the most released rotation energy of magnetar is dominated by GW radiation, we also constrain the upper limit of ellipticity of NS for given EOS, and it is in a range in $[0.89 - 1.8] \times 10^{-3}$. Its GW signal cannot be detected by aLIGO or even for more sensitive Einstein Telescope in the future.

Subject headings: X-rays: burst

1. INTRODUCTION

The merger of a binary neutron star (NS) system is thought to be potential source of producing both gravitational wave (GW) and associated electromagnetic (EM) signals (Berger 2014 for a review). One solid case of producing a GW signal and an associated EM signal (GW 170817 and short GRB 170817A, as well as kilonova AT2017gfo), is already detected by Advanced LIGO, VIRGO, and other telescopes (Abbott et al. 2017; Goldstein et al. 2017; Coulter et al. 2017; Zhang et al. 2018). However, the remnants of a binary NS merger remain an open question.

Depending on the total mass of the system and the poorly known NS equation of state (EOS; Rosswog et al. 2000; Dai et al. 2006; Fan & Xu 2006; Metzger et al. 2010; Rezzolla et al. 2011; Giacomazzo & Perna 2013; Zhang 2013; Lasky et al. 2014; Li et al. 2016), a binary NS merger event can leave with four different types of remnants: (1) a promptly formed black hole (BH; Hotokezaka et al. 2011); (2) a hyper-massive NS, which can survive for ~ 100 ms before collapsing into a BH (Baumgarte et al. 2000; Shibata & Taniguchi 2006; Palenzuela et al. 2015); (3) a supra-massive NS, which is supported by rigid rotation and survives for seconds to hours (Dai et al. 2006; Rowlinson et al. 2010; Hotokezaka et al. 2013; Zhang 2014; Lü et al. 2015; Gao et al. 2016; Kiuchi et al. 2018); (4) a stable NS (Dai & Lu 1998; Zhang & Mészáros 2001; Yu et al. 2010; Metzger et al. 2011;

Bucciantini et al. 2012; Lü & Zhang 2014).

Recently, Xue et al. (2019) discovered an X-ray transient CDF-S XT2 with a host galaxy at redshift $z = 0.738$, to have a moderate offset from the center of the host galaxy and less short GRB associated. Those observational properties are similar to those X-ray features of short GRBs. Such a short-GRB less X-ray transient was predicted by Zhang (2013) and modeled by Sun et al. (2017) before the discovery. Xue et al. (2019) claimed that, the X-ray light curve of CDF-S XT2 is consistent with magnetar central engine model which originates from double neutron star merger. The magnetar parameters in Xue et al. (2019) are inferred by invoking its X-ray plateau and the following decay segment and appear to be consistent with the magnetar parameters in some typical short GRBs. A lower efficiency ($\eta = 0.001$) is adapted to estimate the parameters of magnetar. In such a case, most rotation energy of magnetar may be dissipated in two ways. One is to be transformed into kinetic energy with injecting pulsar wind (Xiao, Zhang & Dai 2019). The other is to be carried away via the strong gravitational wave radiation (Fan et al. 2013; Lasky & Glampedakis 2016; Lü et al. 2018). In this paper, we revisit the X-ray emission of CDF-S XT2, and found that the decay slope after the plateau is more consistent with the prediction of supra-massive NS instead of a stable NS. We consider two scenarios of rotation energy loss of magnetar for post-merger (i.e., EM dominated or GW dominated), and infer the surface magnetic field and initial period of NS, constraining the EOS and ellipticity of NS, as well as detection probability of GW.

This paper is organized as follows. The empirical fitting of X-ray light curve of transient CDF-S XT2 is presented in section 2. The comparisons between CDF-S XT2 and other short GRBs with internal plateau, as well as EOS are discussed in section 3. In section 4, we constrain the ellipticity of NS, and calculate the de-

¹ Guangxi Key Laboratory for Relativistic Astrophysics, Department of Physics, Guangxi University, Nanning 530004, China; lhj@gxu.edu.cn

² School of Astronomy and Space Science, Nanjing University, Nanjing 210093, China

³ Key Laboratory of Modern Astronomy and Astrophysics (Nanjing University), Ministry of Education, Nanjing 210093, China

⁴ Space Science and Technology, Hebei normal university, Shijiazhuang 050000, China

tection probability of GW. The conclusions, along with some discussions, are presented in Section 5. Throughout this paper, a concordance cosmology with parameters $H_0 = 71 \text{ km s}^{-1} \text{ Mpc}^{-1}$, $\Omega_M = 0.30$, and $\Omega_\Lambda = 0.70$ is adapted.

2. LIGHT CURVE FIT AND CENTRAL ENGINE OF CDF-S XT2

2.1. Light curve fit of CDF-S XT2

The X-ray data of CDF-S XT2 observed by Chandra within energy band 0.3-10 keV are taken from Xue et al. (2019). We perform a temporal fit to the light curve with a smooth broken power law model, which is formulated as

$$L = L_0 \left[\left(\frac{t}{t_b} \right)^{\omega\alpha_1} + \left(\frac{t}{t_b} \right)^{\omega\alpha_2} \right]^{-1/\omega} \quad (1)$$

where $t_b = (2525 \pm 242) \text{ s}$ is the break time, $L_b = L_0 \cdot 2^{-1/\omega} = (1.28 \pm 0.16) \times 10^{45} \text{ erg s}^{-1}$ is the luminosity at the break time t_b , $\alpha_1 = (0.09 \pm 0.11)$ and $\alpha_2 = (2.43 \pm 0.19)$ are decay indices before and after the break, respectively. The ω describes the sharpness of the break. The larger the ω parameter, the sharper the break, and $\omega = 3$ is fixed for the light curve fitting. An IDL routine named “mpfitfun.pro” is employed for our fitting (Markwardt 2009). This routine performs a Levenberg-Marquardt least-square fit to the data for a given model to optimize the model parameters.

2.2. Central engine of CDF-S XT2

X-ray transient CDF-S XT2 is located at a star-forming galaxy at redshift $z = 0.738$, lying in the outskirts with a moderate offset from the galaxy center. No significant source-like gamma-ray emission signal was observed above background. Those observed properties are similar to other typical short GRBs (Xue et al. 2019). The estimated event rate density of this event is similar to double NS merger rate density inferred from the detection of GW170817, suggesting that the two are likely from the same origin (Xue et al. 2019). Moreover, the observed X-ray plateau of CDF-S XT2 is consistent with wind dissipation of magnetar central engine, implying that the remnants of such double NS merger should be either supra-massive NS or stable NS. However, our fitting results suggest that the observed stepper decay ($t^{-2.43 \pm 0.19}$) of the X-ray data after the plateau phase is more favored with a supra-massive NS central engine instead of a stable magnetar spin-down model (t^{-2} ; Zhang & Mészáros 2001; Lyons et al. 2010; Rowlinson et al. 2013). The supra-massive NS is unstable and will further collapse into a black hole after thousands of seconds.

To compare the properties of CDF-S XT2 with other short GRBs with internal plateau, Fig. 1 shows the correlation between break luminosity (L_b) and collapse time ($\tau_{\text{col}} = t_b/(1+z)$), as well as the distributions of L_b and τ_{col} . We find that the CDF-S XT2 fall into the 2σ deviation in $L_b - \tau_{\text{col}}$ diagram, suggesting that the other short GRBs with internal plateau samples share the similar central engine with the CDF-S XT2. However, the distributions of luminosity and collapse time of the CDF-S XT2 are much lower and longer than other short GRBs with internal plateau samples. This may be

caused by some observational effects (e.g., on- and off-axis with short GRBs and the CDF-S XT2), or being from different populations of magnetars.

The evidence above points to the supra-massive NS central engine of CDF-S XT2 collapsing into a black hole before it is spin-down. One interesting question is what the energy loss channel of the rotating magnetar is. Is it dominated by the magnetic dipole radiation or gravitational-wave radiation? We will discuss more details for the rotation energy loss of magnetar dominated by EM or GW radiation.

3. THE ROTATION ENERGY LOSS OF MAGNETAR VIA EM EMISSION

3.1. The derived parameters of magnetar

The energy reservoir of a millisecond magnetar is the total rotation energy, which can be written as

$$E_{\text{rot}} = \frac{1}{2} I \Omega^2 \simeq 2 \times 10^{52} \text{ erg } M_{1.4} R_6^2 P_{-3}^{-2}, \quad (2)$$

where I , R , and M are corresponding to the moment of inertia, radius, and mass of the neutron star, respectively. Ω and P are the angular frequency and rotating period of the neutron star, respectively. The convention $Q = 10^x Q_x$ in cgs units is adapted. A magnetar spinning down loses its rotational energy via both magnetic dipole torques (L_{EM}) and GW (L_{GW}) radiations (Zhang & Mészáros 2001; Fan et al. 2013; Giacomazzo & Perna 2013; Lasky & Glampedakis 2016; Lü et al. 2018),

$$\begin{aligned} -\frac{dE_{\text{rot}}}{dt} &= -I\Omega\dot{\Omega} = L_{\text{total}} = L_{\text{EM}} + L_{\text{GW}} \\ &= \frac{B_p^2 R^6 \Omega^4}{6c^3} + \frac{32GI^2 \epsilon^2 \Omega^6}{5c^5}, \end{aligned} \quad (3)$$

where $\epsilon = 2(I_{xx} - I_{yy})/(I_{xx} + I_{yy})$ is the ellipticity describing how large of the neutron star deformation, and B_p is the surface magnetic field at the pole. $\dot{\Omega}$ is the time derivative of the angular frequency. One can find that for a magnetar with given radius and moment of inertia, its L_{EM} depends on B_p and Ω , and L_{GW} depends on ϵ and Ω .

If the rotation energy loss of magnetar is dominated by EM emission, one has

$$L_{\text{EM}} \simeq -I\Omega\dot{\Omega} = \frac{\eta B_p^2 R^6 \Omega^4}{6c^3}. \quad (4)$$

where η is the efficiency of converting the magnetar wind energy into X-ray radiation. The characteristic spin-down luminosity ($L_{\text{EM, sd}}$) and time scale ($\tau_{\text{EM, sd}}$) of magnetar can be expressed as,

$$\begin{aligned} L_{\text{EM, sd}} &= \frac{\eta B_p^2 R^6 \Omega_0^4}{6c^3} \\ &\simeq 1.0 \times 10^{46} \text{ erg s}^{-1} (\eta_{-3} B_{p,15}^2 P_{0,-3}^{-4} R_6^6), \end{aligned} \quad (5)$$

$$\begin{aligned} \tau_{\text{EM, sd}} &= \frac{3c^3 I}{B_p^2 R^6 \Omega_0^2} \\ &\simeq 2.05 \times 10^3 \text{ s } (I_{45} B_{p,15}^{-2} P_{0,-3}^2 R_6^{-6}), \end{aligned} \quad (6)$$

where Ω_0 and P_0 are initial angular frequency and period at $t = 0$, respectively.

Within the magnetar central engine scenario, the observed plateau luminosity is closed to L_b , which is roughly equal to $L_{EM,sd}$, and $\tau_{EM,sd} > \tau_{col}$. One can derive the magnetar parameters B_p and P_0 ,

$$B_{p,15} = 2.05(\eta_{-3}^{1/2} I_{45} R_6^{-3} L_{EM,sd,46}^{-1/2} \tau_{EM,sd,3}^{-1}) \text{ G}, \quad (7)$$

$$P_{0,-3} = 1.42(\eta_{-3}^{1/2} I_{45}^{1/2} L_{EM,sd,46}^{-1/2} \tau_{EM,sd,3}^{-1/2}) \text{ s}. \quad (8)$$

As radiation efficiency η depends strongly on the injected luminosity and wind saturation Lorentz factor (Xiao, Dai & Zhang 2019). By adopting the lower limit of $\tau_{EM,sd}$, we derive the upper limits of P_0 and B_p with different η values. One has $P_0 < 3.4 \times 10^{-3}$ s and $B_p < 4 \times 10^{15}$ G for $\eta = 0.001$, $P_0 < 10.6 \times 10^{-3}$ s and $B_p < 1.2 \times 10^{16}$ G for $\eta = 0.01$, and $P_0 < 33.8 \times 10^{-3}$ s and $B_p < 4 \times 10^{16}$ G for $\eta = 0.1$. Figure 2 shows the $B_p - P_0$ diagram for X-ray transient CDF-S XT2 with different η values, and compares with other short GRBs with internal plateau samples taken from Lü et al. (2015). It seems that the required small P_0 of supra-massive magnetar is needed lower radiation efficiency, and estimated B_p of CDF-S XT2 is lower than other typical short GRBs samples for smaller P_0 . It may be either observational effects (off-axis observations of CDF-S XT2) or different population of magnetars.

3.2. Equation of state of NS

The inferred collapsing time can be used to constrain the neutron star EOS (Lasky et al. 2014; Ravi & Lasky 2014; Lü et al. 2015). The basic formalism is as follows.

The standard dipole spin-down formula gives (Shapiro & Teukolsky 1983)

$$\begin{aligned} P(t) &= P_0 \left(1 + \frac{4\pi^2 B_p^2 R^6}{3c^3 I P_0^2} t\right)^{1/2} \\ &= P_0 \left(1 + \frac{t}{\tau_{EM,sd}}\right)^{1/2}. \end{aligned} \quad (9)$$

The maximum NS mass for a non-rotating NS (M_{TOV}) can be derived for given EOS of NS. The maximum gravitational mass (M_{max}) depends on spin period, read as (Lyford et al. 2003)

$$M_{max} = M_{TOV} (1 + \hat{\alpha} P^{\hat{\beta}}) \quad (10)$$

where $\hat{\alpha}$, $\hat{\beta}$, and M_{TOV} are dependent on the EOS of NS.

As the neutron star spins down, the centrifugal force can no longer sustain the star, and the NS will collapse into a black hole. By using Equation(9) and (10), one can derive the collapse time as function of M_p ,

$$\begin{aligned} t_{col} &= \frac{3c^3 I}{4\pi^2 B_p^2 R^6} \left[\left(\frac{M_p - M_{TOV}}{\hat{\alpha} M_{TOV}} \right)^{2/\hat{\beta}} - P_0^2 \right] \\ &= \frac{\tau_{EM,sd}}{P_0^2} \left[\left(\frac{M_p - M_{TOV}}{\hat{\alpha} M_{TOV}} \right)^{2/\hat{\beta}} - P_0^2 \right]. \end{aligned} \quad (11)$$

Here, we consider 12 EOS that are reported in the literatures (Lasky et al. 2014; Ravi & Lasky 2014; Li et al. 2016; Ai et al. 2018). The basic parameters of those EOS are shown in Table 1.

As noted, one can infer P_0 and B_p by adopting $\eta = 0.001$, and t_{col} from the light curve fit. Following the method of Lasky et al. (2014), tight mass distribution of our Galactic binary NS population is adopted (e.g., Valentim et al. 2011; Kiziltan et al. 2013), and one can infer the expected distribution of proto-magnetar mass, which is found to be $M_p = 2.46_{-0.15}^{+0.13} M_\odot$. For X-ray transient CDF-S XT2, the lower limit of $\tau_{EM,sd} = t_{col}$ is derived. Figure 3 presents the collapse time (t_{col}) as a function of protomagnetar mass (M_p) for CDF-S XT2 with different EOS. Our results show that the GM1, DD2, and DDME2 models give an M_p band falling within the 2σ region of the protomagnetar mass distribution so that the correct EOS should be close to those three models. The maximum mass for non-rotating NS in those three models are $M_{TOV} = 2.37M_\odot$, $2.42M_\odot$, and $2.48M_\odot$, respectively.

4. THE ROTATION ENERGY LOSS OF MAGNETAR VIA GW RADIATION

A survived supra-massive NS central engine requires a more fast spinning ($P_0 \sim 1$ ms) to support the gravitational force (Fan et al. 2013; Gao et al. 2013; Yu et al. 2013; Zhang 2013; Ho 2016; Lasky & Glampedakis 2016). As mentioned above, the estimated periods of magnetar are considerably longer ($\eta = 0.01$ and 0.1) than that expected in the double neutron star merger model. It seems that η should be as low as 0.001 or even smaller to obtain a lower period of a magnetar. If this is the case, the rotation energy loss of magnetar is either transformed to kinetic energy of outflow or dominated by GW radiation. Xiao, Zhang & Dai (2019) present more details for the first situation. In this section, we focus on the other possibility that the most rotation energy of magnetar is dissipated via GW radiation.

4.1. Constraining the ellipticity of NS

Within GW dominated scenario, one has (Lü et al. 2018),

$$L_{GW} \simeq -I\Omega\dot{\Omega} = \frac{32GI^2\epsilon^2\Omega^6}{5c^5}. \quad (12)$$

The characteristic spin-down luminosity ($L_{GW,sd}$) and time scale ($\tau_{GW,sd}$) of NS can be given as,

$$\begin{aligned} L_{GW,sd} &= \frac{32GI^2\epsilon^2\Omega_0^6}{5c^5} \\ &\simeq 1.08 \times 10^{48} \text{ erg s}^{-1} (I_{45}^2 \epsilon_{-3}^2 P_{0,-3}^{-6}), \end{aligned} \quad (13)$$

$$\begin{aligned} \tau_{GW,sd} &= \frac{5c^5}{128GI\epsilon^2\Omega_0^4} \\ &\simeq 9.1 \times 10^3 \text{ s} (I_{45}^{-1} \epsilon_{-3}^{-2} P_{0,-3}^4). \end{aligned} \quad (14)$$

The supra-massive NS of CDF-S XT2 has collapse into black hole before it is spin-down, so that one has $\tau_{GW,sd} > \tau_{col}$. Combining with Equation (14), the upper limit of ellipticity (ϵ) can be expressed as

$$\epsilon < 2.5 \times 10^{-3} I_{45}^{-1/2} P_{0,-3}^2. \quad (15)$$

By fixed $P_0 = 1$ ms, the maximum value of ϵ with different EOS are shown in Table 1. We find that those

values are in the range of $[0.89 - 1.8] \times 10^{-3}$. Those upper limit values are larger than the maximum elastic quadrupole deformation of conventional neutron stars, but are comparable to the upper limit derived for crystalline colour-superconducting quark matter (Lin 2007; Johnson-McDaniel & Owen 2014).

4.2. Detection Probability of a GW

If most of the rotation energy is released via GW radiation with a frequency f , the GW strain for a rotating neutron star at distance D_L can be expressed as,

$$h(t) = \frac{4GI\epsilon}{D_L c^4} \Omega(t)^2. \quad (16)$$

The characteristic amplitude of GW from a rotating NS can be estimated as (Corsi & Mészáros 2009; Hild et al. 2011; Lü et al. 2017),

$$h_c = fh(t) \sqrt{\frac{dt}{df}} = \frac{f}{D_L} \sqrt{\frac{5GI}{2c^3 f}} \\ \approx 8.22 \times 10^{-24} \left(\frac{I}{10^{45} \text{ g cm}^2} \frac{f}{1 \text{ kHz}} \right)^{1/2} \left(\frac{D_L}{100 \text{ Mpc}} \right)^{-1}. \quad (17)$$

For X-ray transient CDF-S XT2, its redshift $z = 0.738$ corresponds to $D_L \sim 4480$ Mpc. By adopting $f = 1000$ Hz, one can estimate the maximum value of the strain h_c for different EOS of NS. The estimated values of h_c are reported in Table 1. The maximum value of the strain h_c for NL3 $\omega\rho$ is about 5×10^{-25} , which is about one order of magnitude smaller than the advanced-LIGO sensitivity, and also less than more sensitive Einstein Telescope (ET; see Figure 4). It means that even if the merger remnant of double NS of this transient is a millisecond massive NS, the post-merger GW signal is undetectable when the rotation energy of the NS is taken away by the GW radiation.

5. CONCLUSIONS AND DISCUSSION

The observed evidence supports that the progenitor of CDF-S XT2 is likely from double NS merger, and the remnants of such double NS merger should be either supra-massive NS or stable NS. Xiao, Zhang & Dai (2019) proposed that both the light curve and spectral evolution of CDF-S XT2 can be well explained by the internal gradual magnetic dissipation process in an ultra-relativistic wind. In this work, we revisit the X-ray emission of CDF-S XT2, and find that the observed step-

per decay of the X-ray light curve after plateau phase of transient CDF-S XT2 is more likely consistent with a supra-massive NS instead of a stable magnetar spin-down model. The supra-massive NS can be survived thousands of seconds before its collapse into a black hole. To compare the observed properties of X-ray emission between CDF-S XT2 and other short GRBs with internal plateau, we show the correlation between break luminosity and collapse time, as well as their distributions. We find that the CDF-S XT2 fall into the 2σ deviation in $L_b - \tau_{\text{col}}$ diagram, suggesting that the other short GRBs with internal plateau samples share a similar central engine type with the CDF-S XT2. However, the distributions of luminosity and collapse time of the CDF-S XT2 is much lower and longer than other short GRBs with internal plateau samples, respectively. It may be caused by some observational effects or from different populations of magnetars.

Moreover, we considered two channels of rotation energy loss of supra-massive magnetar, one is EM dominated, and the other is GW dominated. Within the first scenario, we constrain the EOS of NS by invoking the collapse time, and find that three EOS (GM1, DD2, and DDME2) are consistent with the observational data of CDF-S XT2. We also estimate the parameters of magnetar (i.e., B_p and P_0) for given different radiation efficiency. It seems that the estimated B_p of CDF-S XT2 with lower radiation efficiency is lower than other typical short GRBs samples. It indicate that the most rotation energy may be dissipated via GW radiation. So that, one consider the second scenario of GW dominated. Then, we constrain the upper limit of ellipticity of NS for given different EOS, which is in the range of $[0.89 - 1.8] \times 10^{-3}$. By calculating the possible GW radiation for different EOS, we find that its GW radiation cannot be detected by aLIGO or even for more sensitive Einstein Telescope in the future.

We thank Bing Zhang for helpful comments. This work is supported by the National Natural Science Foundation of China (Grant Nos.11603006, 11851304, 11533003 and 11833003), the Guangxi Science Foundation (grant No. 2017GXNSFFA198008, 2016GXNSFCB380005 and AD17129006). The One-Hundred-Talents Program of Guangxi colleges, Bagui Young Scholars Program, the high level innovation team and outstanding scholar program in Guangxi colleges, and special funding for Guangxi distinguished professors (Bagui Yingcai & Bagui Xuezhe). BBZ is also supported by the National Key Research and Development Program of China (Grant No. 2017YFA0402600) and the National Thousand Young Talents program of China.

REFERENCES

- Abbott, B. P., Abbott, R., Abbott, T. D., et al. 2017, ApJ, 848, L13
 Ai, S., Gao, H., Dai, Z.-G., et al. 2018, ApJ, 860, 57
 Baumgarte, T. W., Shapiro, S. L., & Shibata, M. 2000, ApJ, 528, L29
 Berger, E. 2014, ARA&A, 52, 43
 Bucciantini, N., Metzger, B. D., Thompson, T. A., & Quataert, E. 2012, MNRAS, 419, 1537
 Corsi, A., & Mészáros, P. 2009, ApJ, 702, 1171
 Coulter, D. A., Foley, R. J., Kilpatrick, C. D., et al. 2017, Science, 358, 1556
 Dai, Z. G., & Lu, T. 1998, A&A, 333, L87
 Dai, Z. G., Wang, X. Y., Wu, X. F., & Zhang, B. 2006, Science, 311, 1127
 Fan, Y.-Z., Wu, X.-F., & Wei, D.-M. 2013, Phys. Rev. D, 88, 067304
 Fan, Y.-Z., & Xu, D. 2006, MNRAS, 372, L19
 Gao, H., Ding, X., Wu, X.-F., Zhang, B., & Dai, Z.-G. 2013, ApJ, 771, 86
 Gao, H., Zhang, B., & Lü, H.-J. 2016, Phys. Rev. D, 93, 044065
 Giacomazzo, B., & Perna, R. 2013, ApJ, 771, L26
 Goldstein, A., Veres, P., Burns, E., et al. 2017, ApJ, 848, L14
 Hild, S., Abernathy, M., Acernese, F., et al. 2011, Classical and Quantum Gravity, 28, 094013

- Ho, W. C. G. 2016, *MNRAS*, 463, 489
- Hotokezaka, K., Kyutoku, K., Okawa, H., Shibata, M., & Kiuchi, K. 2011, *Phys. Rev. D*, 83, 124008
- Hotokezaka, K., Kyutoku, K., Tanaka, M., et al. 2013, *ApJ*, 778, L16
- Johnson-McDaniel, N. K., & Owen, B. J. 2013, *Phys. Rev. D*, 88, 044004
- Kiuchi, K., Kyutoku, K., Sekiguchi, Y., & Shibata, M. 2018, *Phys. Rev. D*, 97, 124039
- Kiziltan, B., Kottas, A., De Yoreo, M., & Thorsett, S. E. 2013, *ApJ*, 778, 66
- Lü, H.-J., & Zhang, B. 2014, *ApJ*, 785, 74
- Lü, H.-J., Zhang, B., Lei, W.-H., Li, Y., & Lasky, P. D. 2015, *ApJ*, 805, 89
- Lü, H.-J., Zhang, H.-M., Zhong, S.-Q., et al. 2017, *ApJ*, 835, 181
- Lü, H.-J., Zou, L., Lan, L., & Liang, E.-W. 2018, *MNRAS*, 480, 4402
- Lasky, P. D., & Glampedakis, K. 2016, *MNRAS*, 458, 1660
- Lasky, P. D., Haskell, B., Ravi, V., Howell, E. J., & Coward, D. M. 2014, *Phys. Rev. D*, 89, 047302
- Lattimer, J. M., & Prakash, M. 2004, *Science*, 304, 536
- Li, A., Zhang, B., Zhang, N.-B., et al. 2016, *Phys. Rev. D*, 94, 083010
- Lin, L.-M. 2007, *Phys. Rev. D*, 76, 081502
- Lyford, N. D., Baumgarte, T. W., & Shapiro, S. L. 2003, *ApJ*, 583, 410
- Lyons, N., O'Brien, P. T., Zhang, B., et al. 2010, *MNRAS*, 402, 705
- Markwardt, C. B. 2009, *Astronomical Data Analysis Software and Systems XVIII*, 411, 251
- Metzger, B. D., Giannios, D., Thompson, T. A., Bucciantini, N., & Quataert, E. 2011, *MNRAS*, 413, 2031
- Metzger, B. D., Martínez-Pinedo, G., Darbha, S., et al. 2010, *MNRAS*, 406, 2650
- Palenzuela, C., Liebling, S. L., Neilsen, D., et al. 2015, *Phys. Rev. D*, 92, 044045
- Ravi, V., & Lasky, P. D. 2014, *MNRAS*, 441, 2433
- Rezzolla, L., Giacomazzo, B., Baiotti, L., et al. 2011, *ApJ*, 732, L6
- Rosswog, S., Davies, M. B., Thielemann, F.-K., & Piran, T. 2000, *A&A*, 360, 171
- Rowlinson, A., O'Brien, P. T., Metzger, B. D., Tanvir, N. R., & Levan, A. J. 2013, *MNRAS*, 430, 1061
- Rowlinson, A., O'Brien, P. T., Tanvir, N. R., et al. 2010, *MNRAS*, 409, 531
- Shapiro, S. L., Teukolsky, S. A., & Lightman, A. P. 1983, *Physics Today*, 36, 89
- Shapiro, S. L., & Teukolsky, S. A. 1983, *Research supported by the National Science Foundation*. New York, Wiley-Interscience, 1983, 663 p.
- Shibata, M., & Taniguchi, K. 2006, *Phys. Rev. D*, 73, 064027
- Sun, H., Zhang, B., & Gao, H. 2017, *ApJ*, 835, 7
- Valentim, R., Rangel, E., & Horvath, J. E. 2011, *MNRAS*, 414, 1427
- Xiao, D., Dai, Z.-G., & Zhang, B.-B. 2019, arXiv:1903.09349
- Xiao, D., Zhang, B.-B., & Dai, Z.-G. 2019, arXiv:1903.05480
- Xue, Y.-Q., Zheng, X.-C., Li, Y., et al. 2019, *Nature*, 568, 198
- Yu, Y.-W., Cheng, K. S., & Cao, X.-F. 2010, *ApJ*, 715, 477
- Yu, Y.-W., Zhang, B., & Gao, H. 2013, *ApJ*, 776, L40
- Zhang, B.-B., Zhang, B., Sun, H., et al. 2018, *Nature Communications*, 9, 447
- Zhang, B. 2014, *ApJ*, 780, L21
- Zhang, B. 2013, *ApJ*, 763, L22
- Zhang, B., & Mészáros, P. 2001, *ApJ*, 552, L35

TABLE 1
THE BASIC PARAMETERS OF EOS OF NS

	$M_{TOV}(M_{\odot})$	R (km)	$I(10^{45} \text{ g cm}^2)$	$\hat{\alpha}(10^{-10} \text{ s}^{-\hat{\beta}})$	$\hat{\beta}$	$\epsilon(10^{-3})^a$	$h_c(f)(10^{-25})^b$
BCPM	1.98	9.94	2.86	3.39	-2.65	1.5	3.02
SLy	2.05	9.99	1.91	1.60	-2.75	1.8	2.47
Bsk20	2.17	10.17	3.50	3.39	-2.68	1.3	3.34
Shen	2.18	12.40	4.68	4.69	-2.74	1.2	3.87
APR	2.20	10.0	2.13	0.303	-2.95	1.7	2.61
Bsk21	2.28	11.08	4.37	2.81	-2.75	1.2	3.74
GM1	2.37	12.05	3.33	1.58	-2.84	1.4	3.26
DD2	2.42	11.89	5.43	1.37	-2.88	1.1	4.16
DDME2	2.48	12.09	5.85	1.966	-2.84	1.0	4.32
AB-N	2.67	12.90	4.30	0.112	-3.22	1.2	3.71
AB-L	2.71	13.70	4.70	2.92	-2.82	1.2	3.87
NL3 $\omega\rho$	2.75	12.99	7.89	1.706	-2.88	0.89	5.02

REFERENCES. — The EOS of NS parameters are taken from Lasky et al. (2014), Ravi & Lasky (2014), Li et al. (2016), and Ai et al. (2018).

^a The estimated upper limit of ellipticity with $P_0 = 1$ ms.

^b The maximum value of the strain for GW with $f = 1000\text{Hz}$.

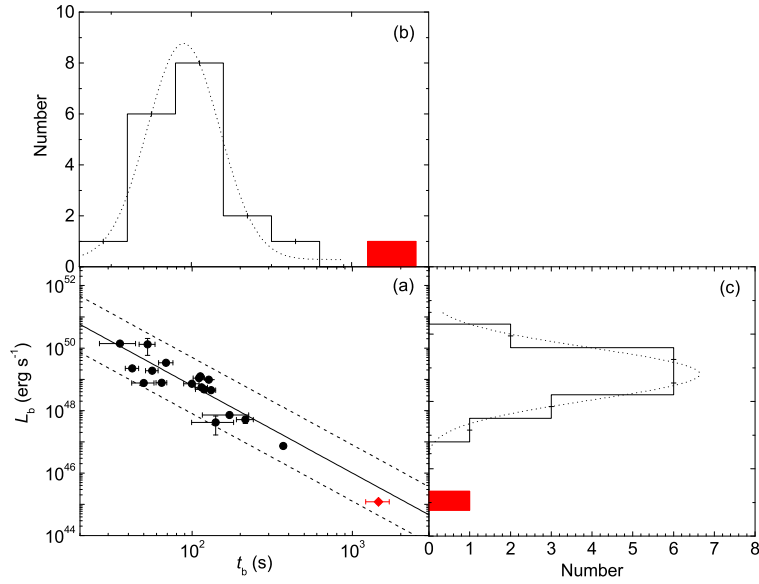


FIG. 1.— (a): X-ray plateau luminosity (L_0) as function of collapse time (t_{col}) for short GRBs with internal plateau (black dots) and X-ray transient CDF-S XT2 (red diamond). The black solid line is the the best fit with power-law model, and the two dashed lines mark the 2σ region of the correlation, respectively. (b) and (c): Distributions of t_{col} and L_0 with best-fit Gaussian profiles, respectively.

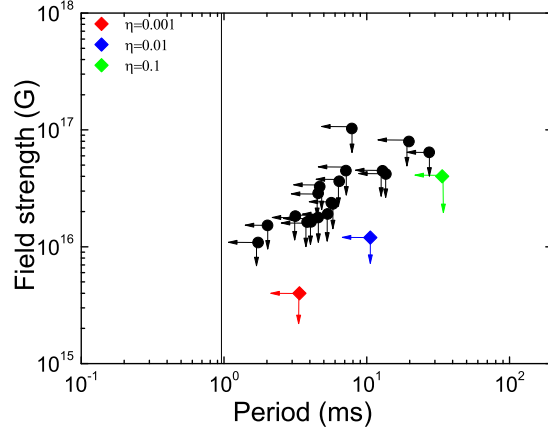


FIG. 2.— Inferred magnetar parameters, initial spin period P_0 vs. surface polar cap magnetic field strength B_p derived for short GRBs with internal plateau (black dots) and X-ray transient CDF-S XT2 (diamond) with $\eta = 0.1, 0.01$ and 0.001 . The vertical solid line is the break-up spin period limit for a neutron star (Lattimer & Prakash 2004).

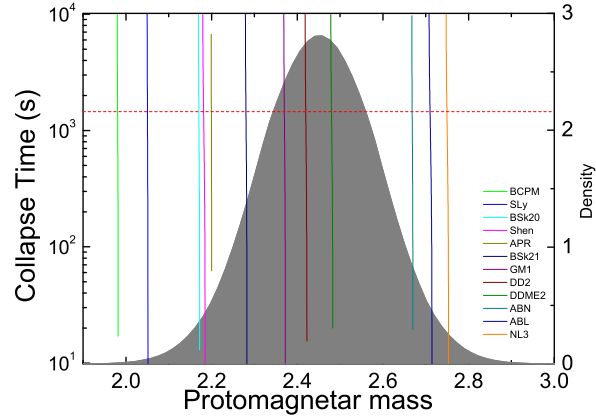


FIG. 3.— Collapse time as a function of the protomagnetar mass of CDF-S XT2 for different EOS (color lines). The shaded region is the protomagnetar mass distribution derived from the total mass distribution of the Galactic NSCNS binary systems. The horizontal dashed line is the collapse time in the rest frame.

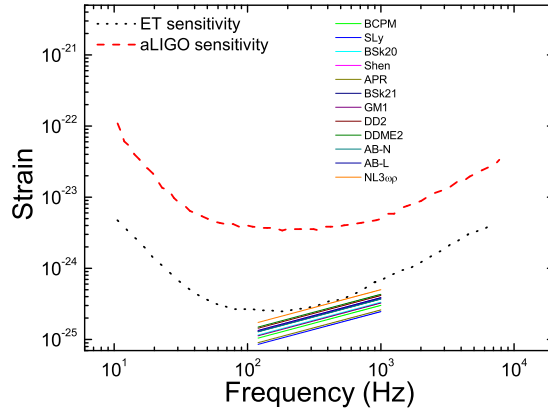


FIG. 4.— Gravitational-wave strain evolution with frequency for CDF-S XT2 with different EOS at distances $D_L = 4480$ Mpc (color lines). The black dotted and red dashed lines are the sensitivity limits for aLIGO and ET, respectively.